Electrophysiology

Brain slices were prepared essentially as described[29]. IPSCs and population spikes were evoked by square pulse stimuli (0.066 Hz, 5–12 mA, 200 μs) delivered by means of bipolar tungsten electrodes positioned within the lateral amygdala close to the external capsule. Population spikes were recorded in the basolateral amygdala close to lateral amygdala using glass microelectrodes (2–3 MΩ) filled with artificial cerebrospinal fluid (ACSF)[29]. HFS (five trains at 100 Hz for 1 s, 10-s interstimulus interval) was applied to induce LTP, and LFS1 (900 pulses at 1 Hz) was applied to induce LTD. Whole-cell GABA-mediated currents were isolated by adding NBQX (0.005 mM) and D-(-)-2-amino-5-phosphopentanoic acid (AP5; 0.05 mM) to ACSF (bubbled with 95% O_2/5% CO_2; pH 7.3), and were recorded from visually identified somata of principal neurons of the basolateral amygdala[30] by glass electrodes (4.5–5 MΩ)[16] containing (in mM): Mg-ATP 2, $CsCH_3SO_3$ 100, CsCl 60, EGTA 0.2, HEPES 10, $MgCl_2$ 1, QX314 5 and Na_3GTP 0.3 (pH 7.3). Patch clamp experiments were performed at 24 ± 1 °C at a holding potential of −70 mV. LTD_i was induced by 100 stimuli at 1 Hz (LFS 2). PPF was induced as described[30]. Data are expressed as means ± s.e.m. We tested significance using the Student's *t*-test.

Received 24 December 2001; accepted 16 April 2002; doi:10.1038/nature00839.

1. LeDoux, J. E. Emotion circuits in the brain. *Annu. Rev. Neurosci.* **23,** 155–184 (2000).
2. Davis, M., Falls, W. A. & Gewirtz, J. in *Contemporary Issues in Modeling Psychopathology* (eds Myslobodsky, M. S. & Weiner, I.) 113–141 (Kluwer Academic, Norwell, 2000).
3. Matsuda, L. A., Lolait, S. J., Brownstein, M. J., Young, A. C. & Bonner, T. I. Structure of a cannabinoid receptor and functional expression of the cloned cDNA. *Nature* **346,** 561–564 (1990).
4. Di Marzo, V., Melck, D., Bisogno, T. & De Petrocellis, L. Endocannabinoids: endogenous cannabinoid receptor ligands with neuromodulatory action. *Trends Neurosci.* **21,** 521–528 (1998).
5. Marsicano, G. & Lutz, B. Expression of the cannabinoid receptor CB1 in distinct neuronal subpopulations in the adult mouse forebrain. *Eur. J. Neurosci.* **11,** 4213–4225 (1999).
6. Katona, I. *et al.* Distribution of CB1 cannabinoid receptors in the amygdala and their role in the control of GABAergic transmission. *J. Neurosci.* **21,** 9506–9518 (2001).
7. Hampson, R. E. & Deadwyler, S. A. Role of cannabinoid receptors in memory storage. *Neurobiol. Dis.* **5,** 474–482 (1998).
8. Reibaud, M. *et al.* Enhancement of memory in cannabinoid CB1 receptor knock-out mice. *Eur. J. Pharmacol.* **379,** R1–R2 (1999).
9. Falls, W. A., Miserendino, M. J. & Davis, M. Extinction of fear-potentiated startle: blockade by infusion of an NMDA antagonist into the amygdala. *J. Neurosci.* **12,** 854–863 (1992).
10. Lu, K. T., Walker, D. L. & Davis, M. Mitogen-activated protein kinase cascade in the basolateral nucleus of amygdala is involved in extinction of fear-potentiated startle. *J. Neurosci.* **21,** RC162 (2001).
11. Pertwee, R. G. Cannabinoid receptors and pain. *Prog. Neurobiol.* **63,** 569–611 (2001).
12. Rodriguez de Fonseca, F., Del Arco, I., Martin-Calderon, J. L., Gorriti, M. A. & Navarro, M. Role of the endogenous cannabinoid system in the regulation of motor activity. *Neurobiol. Dis.* **5,** 483–501 (1998).
13. Rinaldi-Carmona, M. *et al.* SR141716A, a potent and selective antagonist of the brain cannabinoid receptor. *FEBS Lett.* **350,** 240–244 (1994).
14. Petitet, F., Jeantaud, B., Bertrand, P. & Imperato, A. Cannabinoid penetration into mouse brain as determined by *ex vivo* binding. *Eur. J. Pharmacol.* **374,** 417–421 (1999).
15. Morgan, M. A., Romanski, L. M. & LeDoux, J. E. Extinction of emotional learning: contribution of medial prefrontal cortex. *Neurosci. Lett.* **163,** 109–113 (1993).
16. Wilson, R. I. & Nicoll, R. A. Endogenous cannabinoids mediate retrograde signalling at hippocampal synapses. *Nature* **410,** 588–592 (2001).
17. Ohno-Shosaku, T., Maejima, T. & Kano, M. Endogenous cannabinoids mediate retrograde signals from depolarized postsynaptic neurons to presynaptic terminals. *Neuron* **29,** 729–738 (2001).
18. Santini, E., Muller, R. U. & Quirk, G. J. Consolidation of extinction learning involves transfer from NMDA-independent to NMDA-dependent memory. *J. Neurosci.* **21,** 9009–9017 (2001).
19. El Ghundi, M., O'Dowd, B. F. & George, S. R. Prolonged fear responses in mice lacking dopamine D1 receptor. *Brain Res.* **892,** 86–93 (2001).
20. Quirk, G. J., Russo, G. K., Barron, J. L. & Lebron, K. The role of ventromedial prefrontal cortex in the recovery of extinguished fear. *J. Neurosci.* **20,** 6225–6231 (2000).
21. Tang, Y. P. *et al.* Genetic enhancement of learning and memory in mice. *Nature* **401,** 63–69 (1999).
22. Harris, J. A. & Westbrook, R. F. Evidence that GABA transmission mediates context-specific extinction of learned fear. *Psychopharmacology (Berl.)* **140,** 105–115 (1998).
23. McGaugh, J. L., Castellano, C. & Brioni, J. Picrotoxin enhances latent extinction of conditioned fear. *Behav. Neurosci.* **104,** 264–267 (1990).
24. Medina, J. F., Repa, C. J., Mauk, M. D. & LeDoux, J. E. Parallels between cerebellum- and amygdala-dependent conditioning. *Nature Rev. Neurosci.* **3,** 122–131 (2002).
25. Collins, D. R. & Paré, D. Reciprocal changes in the firing probability of lateral and central medial amygdala neurons. *J. Neurosci.* **19,** 836–844 (1999).
26. Royer, S., Martina, M. & Paré, D. An inhibitory interface gates impulse traffic between the input and output stations of the amygdala. *J. Neurosci.* **19,** 10575–10583 (1999).
27. Franklin, K. B. J. & Paxinos, G. *The Mouse Brain* (Academic, San Diego, 1997).
28. Di Marzo, V. *et al.* Levels, metabolism, and pharmacological activity of anandamide in CB(1) cannabinoid receptor knockout mice: evidence for non-CB(1), non-CB(2) receptor-mediated actions of anandamide in mouse brain. *J. Neurochem.* **75,** 2434–2444 (2000).
29. Rammes, G. *et al.* Synaptic plasticity in the basolateral amygdala in transgenic mice expressing dominant-negative cAMP response element-binding protein (CREB) in forebrain. *Eur. J. Neurosci.* **12,** 2534–2546 (2000).
30. Rammes, G., Eder, M., Dodt, H.-U., Kochs, E. & Zieglgänsberger, W. Long-term depression in the basolateral amygdala of the mouse involves the activation of interneurons. *Neuroscience* **107,** 85–97 (2001).

Supplementary Information accompanies the paper on *Nature*'s website (http://www.nature.com/nature).

Acknowledgements

S.C.A., T.B. and G.R. contributed equally to this work. We thank S. Bourier, B. Brachvogel and W. Wurst for feeder cells and technical support; K. Pfeffer for E14 embryonic stem cells; K. Rajewsky for Cre deleter mouse line; B. Lüscher for FRT-flanked PGK-neo cassette; M. Wiedemann, H. Dietrich, B. Wölfel, A. Daschner, F. Fezza and A. Rippl for technical assistance, mouse breeding and genotyping; A. Mederer for help with behavioural experiments; F. Holsboer for continuous support; E. Güll for secretarial work; and C. Behl for critically reading the manuscript.

Competing interests statement

The authors declare that they have no competing financial interests.

Correspondence and requests for materials should be addressed to B.L. (e-mail: lutz@mpipsykl.mpg.de).

A transcription factor response element for gene expression during circadian night

Hiroki R. Ueda*†, Wenbin Chen*, Akihito Adachi‡, Hisanori Wakamatsu*, Satoko Hayashi*, Tomohiro Takasugi*, Mamoru Nagano‡ Ken-ichi Nakahama‡, Yutaka Suzuki§, Sumio Sugano§, Masamitsu Iino†, Yasufumi Shigeyoshi‡ & Seiichi Hashimoto*

** Molecular Medicine Laboratories, Institute for Drug Discovery Research, Yamanouchi Pharmaceutical Company, Ltd, 21 Miyukigaoka, Tsukuba, Ibaraki 305-8585, Japan*
† Department of Pharmacology, Graduate School of Medicine, The University of Tokyo, 7-3-1 Bunkyo-ku, Tokyo 113-0033, Japan
‡ Department of Anatomy and Neurobiology, Kinki University School of Medicine, 377-2 Ohno-Higashi, Osakasayama City, Osaka 589-8511, Japan
§ Human Genome Center, Institute of Medical Science, The University of Tokyo, 4-6-1 Shirokane-dai, Minato-ku, Tokyo 108-8639, Japan

Mammalian circadian clocks consist of complex integrated feedback loops[1–10] that cannot be elucidated without comprehensive measurement of system dynamics and determination of network structures[11]. To dissect such a complicated system, we took a systems-biological approach based on genomic, molecular and cell biological techniques. We profiled suprachiasmatic nuclei and liver genome-wide expression patterns under light/dark cycles and constant darkness. We determined transcription start sites of human orthologues for newly identified cycling genes and then performed bioinformatical searches for relationships between time-of-day specific expression and transcription factor response elements around transcription start sites. Here we demonstrate the role of the Rev-ErbA/ROR response element in gene expression during circadian night, which is in phase with *Bmal1* and in antiphase to *Per2* oscillations. This role was verified using an *in vitro* validation system, in which cultured fibroblasts transiently transfected with clock-controlled reporter vectors exhibited robust circadian bioluminescence[12].

To perform comprehensive measurement of mammalian circadian gene expression, we profiled genome-wide expression patterns of central (suprachiasmatic nuclei, SCN) and peripheral (liver) clocks every four hours during light/dark cycles (LD) or constant darkness (DD) over two days. We extracted total RNA from 50 pooled SCNs and four pooled livers at each time point, prepared biotinylated complementary RNA and used an Affymetrix mouse high-density oligonucleotide probe array (GeneChip) to determine SCN and liver gene expression.

The data obtained were analysed through two statistical cosine filters, one for LD and the other for DD time courses (see

Supplementary Information), to identify a set of genes rhythmically expressed under both LD and DD. On the basis of two successive filtrations, we classified 101 genes in the SCN and 393 genes in the liver as 'significantly rhythmic under both LD and DD'. In addition, we found two genes in the liver, *Rgs16* and *Hsp70-1*, with high 24-h autocorrelation under LD and DD and high cross-correlation between LD and DD liver expression profiles (see Supplementary Information), but without high correlation with the cosine curves. In total, we identified 101 genes in the SCN and 395 genes in the liver (Supplementary Information Tables 1 and 2). We also found 21 genes rhythmically expressed in both tissues (Supplementary Information Table 3). These are likely to be the minimum numbers of genes rhythmically expressed under both LD and DD in the SCN and/or liver; the number may increase if different filtration cut-off values are applied. Random profiles produced 18 and 13 samples classified as 'rhythmic under both LD and DD' in the SCN and liver, respectively. Using this estimate, we concluded that we had identified a substantial number (~80 for the SCN and ~380 for the liver) of cycling genes.

Figures 1b and 2b display the cycling genes that we identified from the SCN and liver expression profiles, ordered by the averaged peak time between LD and DD (see Supplementary Information). Peak times of periodic expression profiles are spread over 24 h. When classified into 4-h interval groups ranging from CT0 (circadian time zero: the beginning of the subjective day) to CT24 (the end of subjective night, equal to CT0), we found the following distribution of peak times in the SCN (Supplementary Information Table 1): eight genes in CT0–4, 23 genes in CT4–8, 16 genes in CT8–12, 16 genes in CT12–16, 28 genes in CT16–20 and ten genes in CT20–24. We also found the following distribution in the liver (Supplementary Information Table 2): 91 genes in CT0–4, 71 genes in CT4–8, 58 genes in CT8–12, 63 genes in CT12–16, 50 genes in CT16–20 and 54 genes in CT20–24. The locations of these groups are indicated in Figs 1b and 2b.

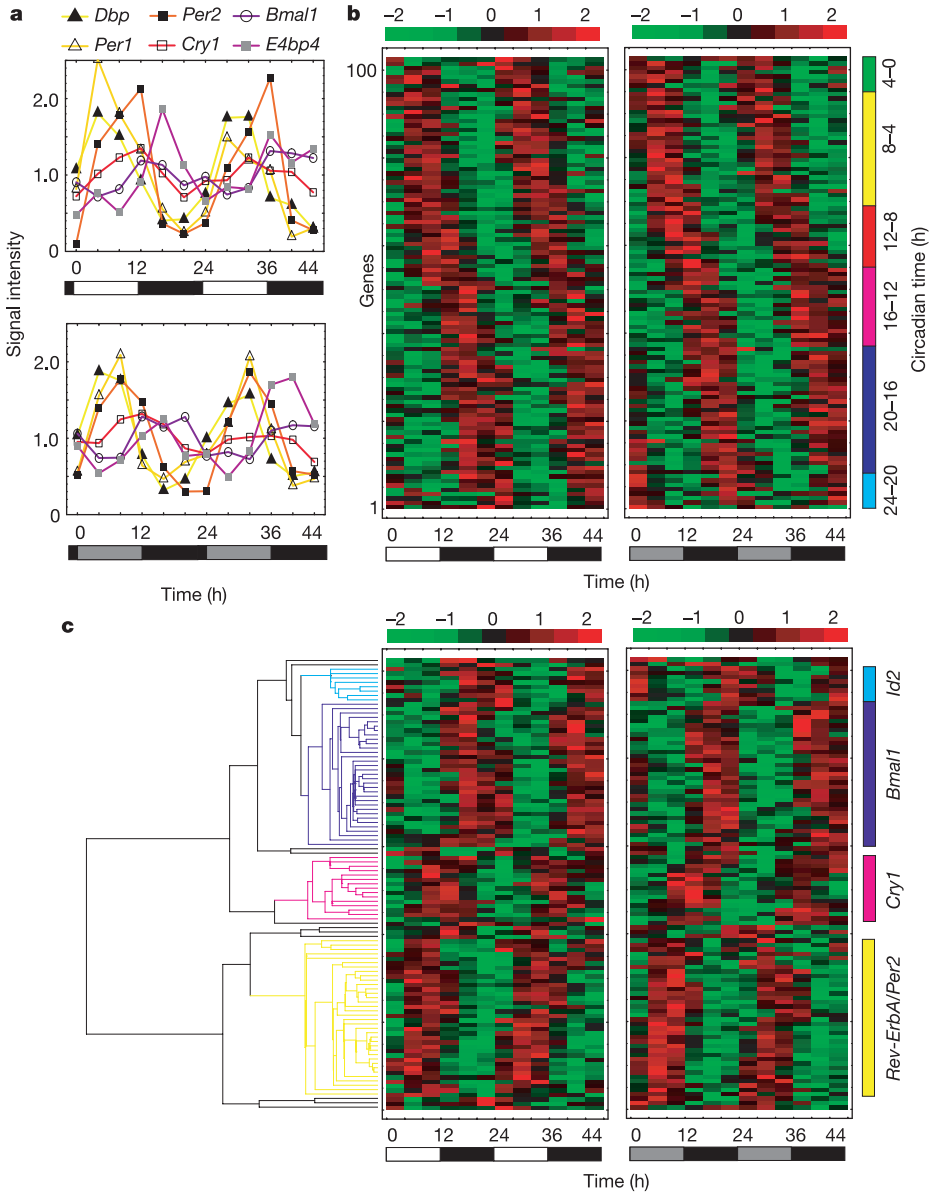

Figure 1 Temporal expression profiles in mouse suprachiasmatic nuclei. **a**, Periodic expression of known clock-controlled genes in mouse SCN under light/dark cycles (LD) and constant darkness (DD). Data were normalized so that the average signal intensity over 12-point time courses is 1.0. **b**, **c**, Organization of SCN expression profiles by peak time (**b**) and hierarchical clustering (**c**). In both diagrams, columns represent time points, and rows represent genes. The colours in descending order from red to black to green represent the normalized data (the average and standard deviation over 12-point time courses are 0.0 and 1.0, respectively).

To cluster our cycling genes in accordance with the data, we performed hierarchical clustering. Figures 1c and 2c display the entire organization of our cycling genes in the SCN and liver, respectively. We found four main clusters in the SCN: the *Rev-ErbA/Per2* cluster (35 genes, average phase at CT6.0), *Cry1* cluster (15 genes, average phase at CT12.1), *Bmal1* cluster (32 genes, average phase at CT17.0) and *Id2* cluster (eight genes, average phase at CT20.8). We also found five main clusters in the liver: the *Rev-ErbA* cluster (87 genes, average phase at CT8.0), *Per2* cluster (75 genes, average phase at CT13.2), *Cry1* cluster (52 genes, average phase at CT17.8), *Bmal1* cluster (58 genes, average phase at CT20.5) and *Id* cluster (107 genes, average phase at CT3.1). The locations of these clusters are indicated in Figs 1c and 2c (see Supplementary Information Figs 1 and 2 for detailed results).

As an independent test, we measured the levels of expression under DD of three to 12 genes for each cluster using the quantitative polymerase chain reaction (PCR) assay in both SCN and liver. We used the same samples that were used to prepare probes for microarray hybridizations. The expression profiles of the genes, as measured by these two independent methods, were very similar in both phase and amplitude (Supplementary Information Figs 3 and 4). These results confirmed our microarray measurements. To verify further our SCN microarray measurements, we explored the spatiotemporal expression profiles under DD of the genes identified in the SCN by an *in situ* hybridization study using ^{35}S-labelled cRNA probes (Fig. 3). The spatiotemporal expression profiles obtained from the *in situ* hybridization study were highly consistent with the temporal expression pattern obtained from the microarray experiments and further complement the microarray data because their signal intensity in the SCN is difficult to infer from microarray data.

Identification of more than 100 cycling genes in the SCN and nearly 400 cycling genes in the liver offered the opportunity to infer the transcriptional control mechanisms generating circadian expression. To do so, we analysed the promoter regions of newly

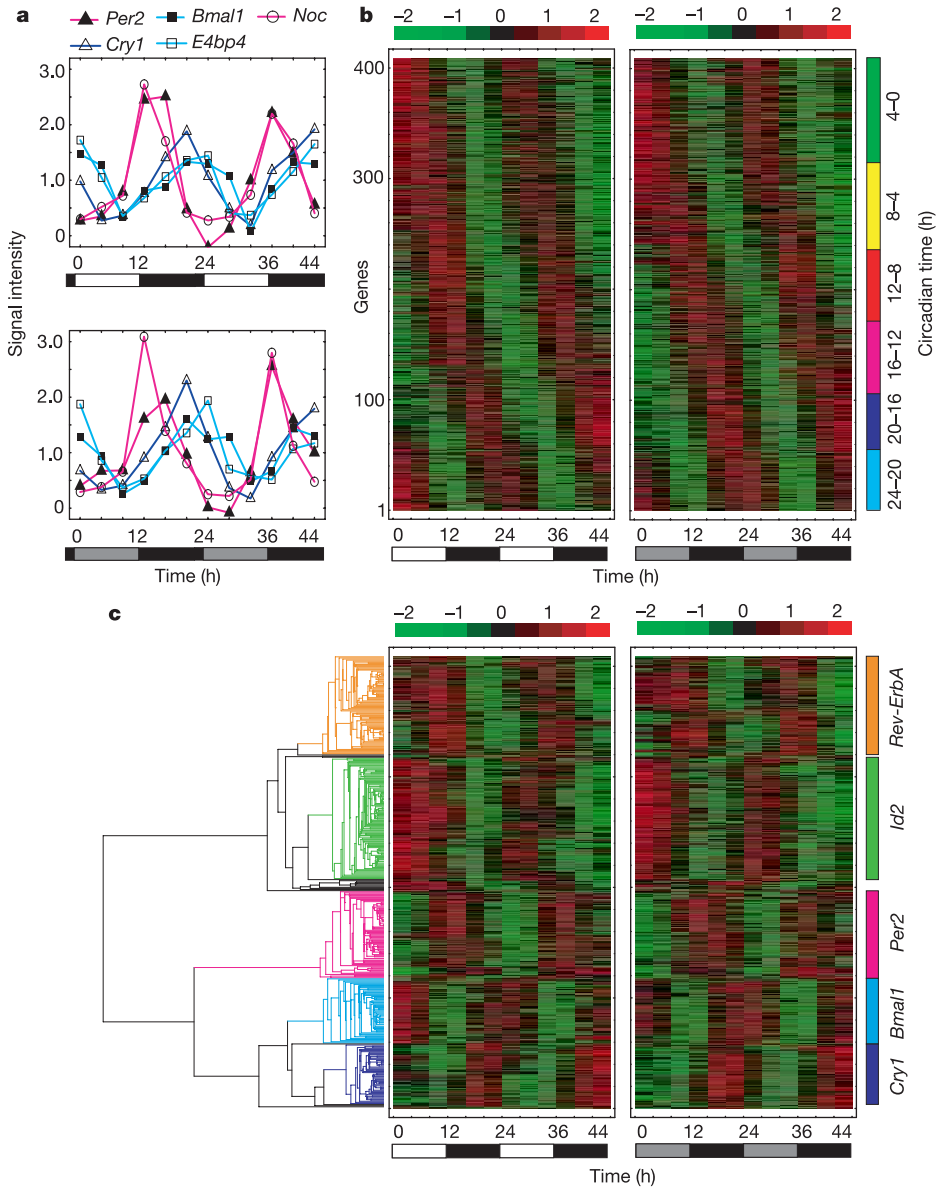

Figure 2 Temporal expression profiles in the mouse liver. **a**, Periodic expression of known clock-controlled genes in mouse liver under LD and DD. Data were normalized so that the average signal intensity over 12-point time courses is 1.0. **b**, **c**, Organization of liver expression profiles by peak time (**b**) and hierarchical clustering (**c**). In both diagrams, columns represent time points, and rows represent genes. The colours in descending order from red to black to green represent the normalized data (the average and standard deviation over 12-point time courses are 0.0 and 1.0, respectively).

identified cycling genes in the SCN and liver. One of the main difficulties in analysing the promoter regions in higher eukaryotes, such as humans, mice and rats, is the lack of precise positional information of transcription start sites (TSSs). It is difficult to use translation start codons to estimate promoter regions because in many cases TSSs appear to be distant from translation initiation sites in higher eukaryotes. In fact, the TSS of the clock gene *Bmal1* is more than 60 kilobases (kb) away from the translation initiation ATG codon[10]. The other difficulty in analysing the promoter regions of mouse genes is the low coverage of publicly available sequence information over the entire mouse genome.

To address these two difficulties, we systematically determined the TSS of human orthologues of newly identified cycling genes by the oligo-capping method[13] (see Methods) and then mapping the TSS onto the human genome, the draft sequence for which is publicly available. This approach is based on the evidence that circadian systems are well conserved between human and mouse[14], and that the promoter region of the clock gene *Per1* is highly homologous in humans and mice[15]. We identified the TSS of 45 and 189 human orthologues for cycling genes in the SCN and liver, respectively (Supplementary Information Tables 4 and 5). Using positional information for these TSSs on the human genome, we defined the adjacent sequences as the putative promoter regions. We then searched for the relationship between circadian expression and known circadian transcription factor response elements in the retrieved promoter regions of these genes (see Supplementary Information Tables 6 and 7 for detailed results).

We found seven cycling genes in the SCN with putative cyclic AMP response elements (CRE: TGACGT[16]) in the promoter regions of their orthologues, the phases of which consolidate to subjective day (circadian time, CT7.0 ± 1.6, mean ± s.d.). Phase consolidation of the genes with putative CRE is consistent with the previous observation that the reporter gene, driven by a CRE-containing promoter, displays clear circadian expression with a peak time occurring during subjective day in the SCN[17].

We also found ten cycling genes in the SCN with putative Rev-ErbA/ROR response elements (AGGTCA[18]), to which Rev-ErbA and ROR family members bind, in the promoter regions of their orthologues. The phases of these genes consolidate to subjective night or dawn (CT19.2 ± 3.3, mean ± s.d.). The ten genes identified include *Bmal1* and *E4bp4*, which display similar circadian expressions antiphase to *Per2* oscillations in both SCN and the liver (Figs 1 and 2). These observations suggest that Rev-ErbA/ROR response elements play an important role in generating circadian oscillation antiphase to *Per* genes expression.

To explore the roles of Rev-ErbA/ROR response elements, we first examined in detail the spatiotemporal expression profiles in the SCN of all entire Rev-ErbA and ROR family members shown to bind to the same Rev-ErbA/ROR response element[19]. *Rev-ErbA*, *Rev-ErbAβ*, *RORα* and *RORβ* displayed similar circadian expression profiles in the SCN, with peaks during the day and troughs during the night (Fig. 4), whereas *RORγ* was not detected in the SCN throughout the 24-h cycle (data not shown). *Rev-ErbAα*, *Rev-ErbAβ* and *RORα* demonstrated dynamic oscillation and were expressed very highly at CT4 (*Rev-ErbAα* and *Rev-ErbAβ*) or CT8 (*RORα*), with peak levels three times those of troughs. *RORβ* showed moderate to strong expression at every time point examined. The amplitude of *RORβ* oscillation was low compared with those of the other three genes in the family.

We also examined in detail the temporal expression profiles in the liver of the entire Rev-ErbA and ROR family by quantitative PCR. *Rev-ErbAα*, *Rev-ErbAβ* and *RORγ* exhibited clear circadian oscillations (Supplementary Information Fig. 5) whereas *RORα* exhibited little or no circadian rhythmicity, and *RORβ* was not detected in the liver throughout the 24-h cycle (data not shown). *Rev-ErbAα* and *Rev-ErbAβ* demonstrated dynamic oscillation, were very highly expressed at CT4–8 (*Rev-ErbAα*) and CT8 (*Rev-ErbAβ*), and had peak levels more than 100 (*Rev-ErbAα*) and ten (*Rev-ErbAβ*) times

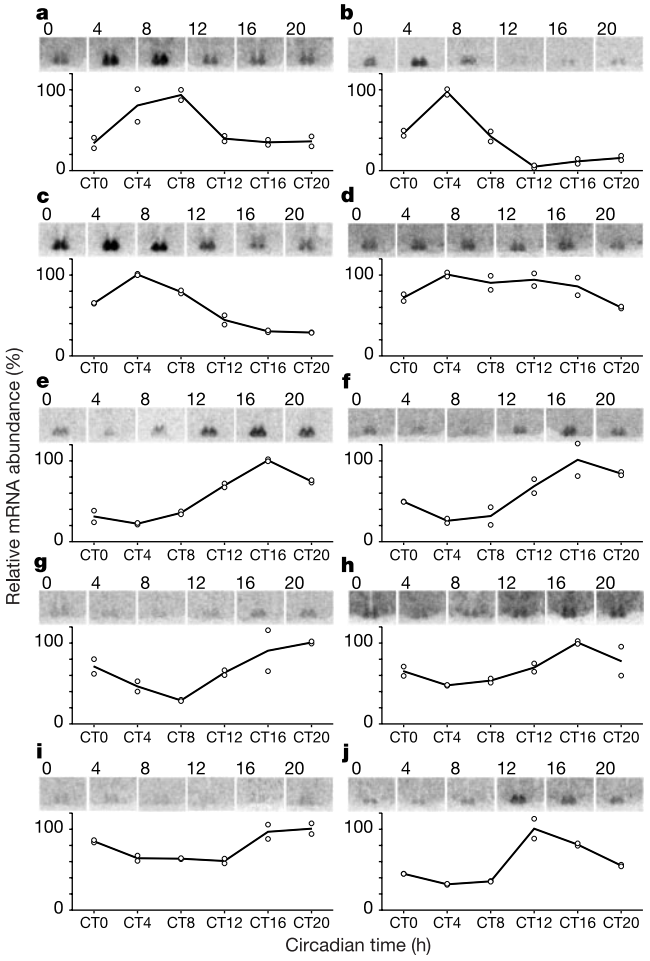

Figure 3 Spatiotemporal expression profiles in mouse SCN under DD conditions. Data for the genes (*Hmg4* (**a**), Ras-like protein *1190017B18Rik* (**b**), *Rgs16* (**c**), Oligoribonuclease-like protein *1810038D15Rik* (**d**), *Dexras1* (**e**), *V1a* (**f**), *Pkiβ* (**g**), *Hsp105* (**h**), *Id2* (**i**) and *Hsp40* (**j**)) consist of representative *in situ* hybridization autoradiograms of the SCN and quantitative graphs. Numbers above the radiograms indicate circadian time (h). Means are indicated by solid lines and individual values by open circles ($n = 2$).

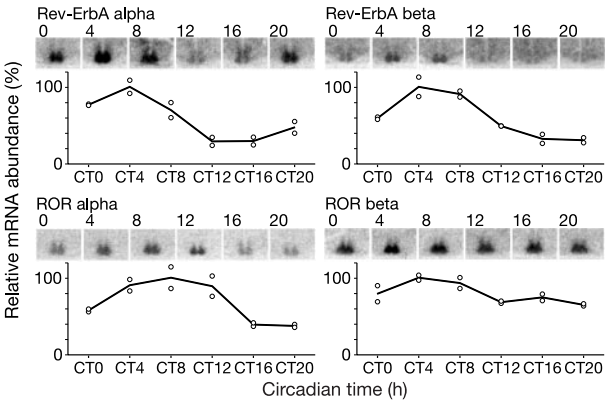

Figure 4 Spatiotemporal profiles of expression of the Rev-ErbA and ROR family in the mouse SCN under DD conditions. Representative *in situ* hybridization autoradiograms and graphs of relative mRNA abundance are shown. Numbers above the radiograms indicate circadian time (h). Means are indicated by solid lines and individual values by open circles ($n = 2$).

trough levels. *RORγ* also displayed clear oscillations, and was expressed highly at CT16–20 with a peak level three times the trough level.

To validate the hypothesized circadian circuit, we have developed an *in vitro* clock-controlled element determination system[12]. We created *dLuc* by fusing a rapid degradation domain modified from mouse ornithine decarboxylase to the carboxy-terminal end of firefly luciferase. The rapid functional half-life of the dLuc proteins, 20–30 min, was suitable for probing circadian transcriptional dynamics in real time[12].

To verify the role of Rev-ErbA/ROR response elements in generating circadian expression antiphase to *Per2* oscillation, we fused the 60-base-pair promoter region of the *Bmal1* promoter, containing wild-type and mutant Rev-ErbA/ROR response elements, to the SV40 basic promoter driving a *dLuc* reporter gene (Fig. 5a). This 60-base-pair region is completely conserved between human and mouse *Bmal1* genes and is near the TSS in both cases. Transfection experiments confirmed that the wild-type construct can be activated by *RORα* and repressed by *Rev-ErbAα*, and that the mutant cannot (data not shown). To examine the circadian expression driven by the Rev-ErbA/ROR response element, we transfected these constructs into cultured Rat1-R12 fibroblasts, stimulated with dexamethasone, and measured luminescence from these cells. Bioluminescence levels from the wild-type Rev-ErbA/ROR response elements displayed circadian rhythmicity (Fig. 5d, $n = 3$) and the phase of their oscillations was in phase with the levels of luminescence from the *Bmal1* promoter fused to the destabilized luciferase (Fig. 5c, $n = 3$) and antiphase to those from the *Per2* promoter (Fig. 5b, $n = 3$). On the other hand, bioluminescence levels from the mutant Rev-ErbA/ROR response elements exhibited no circadian rhythmicity (Fig. 5e, $n = 3$) and displayed light emission patterns similar to those from the *SV40* promoter alone (Fig. 5f, $n = 3$). On the basis of these observations, we concluded that Rev-ErbA/ROR response elements play an important role in generating circadian night expression in phase with *Bmal1* expression and antiphase to *Per2* expression.

We have thus analysed mammalian circadian rhythms on the basis of genome-wide expression measurements, extensive determination of TSSs, bioinformatical search for transcription factor response elements, and *in vitro* validation of clock-controlled elements. The power of this systems-biological approach is demonstrated by the discovery and validation of the function of Rev-ErbA/ROR response elements in generating gene expression during circadian night, which is in phase with *Bmal1* and antiphase to *Per2* expression. This approach can be applied to the analysis of recently described mammalian cycling genes[20–24]. Although efficient *in vitro* validation systems remain to be developed, the systems-biological approach may be applicable to circadian rhythms in higher eukaryotes such as *Drosophila*[25–27] or *Arabidopsis*[28], as well as other biological systems such as mammalian cell cycles[29], in which genome-wide expression profiles have been measured. □

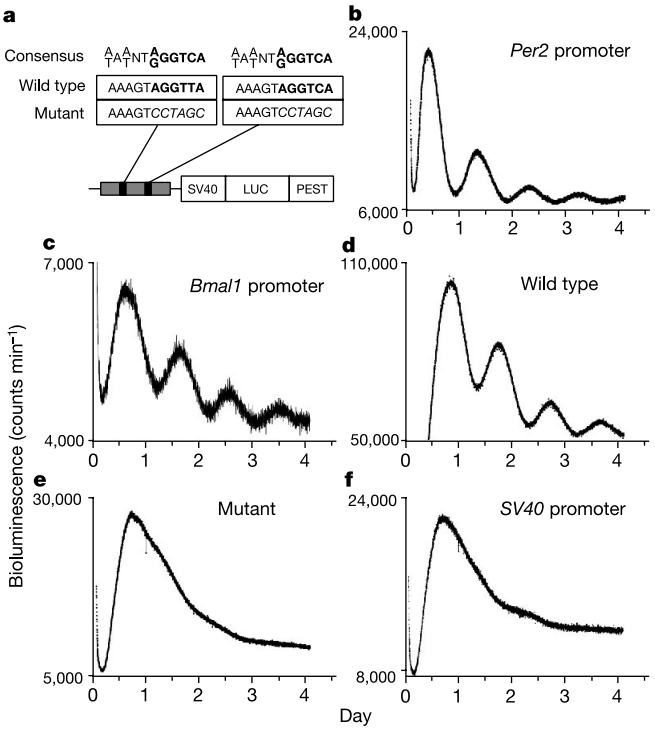

Figure 5 A Rev-ErbA/ROR response element sufficient for gene expression during circadian night. **a**, Diagram of wild-type and mutant 60-base-pair *Bmal1* promoter region fused to the SV40 basic promoter driving a destabilized luciferase (*dLuc*) reporter gene. The wild-type 60-base-pair region contains two putative Rev-ErbA/ROR response elements. Well-conserved base pairs[18] (bold) and mutated base pairs (italic) are indicated. **b**, **c**, Representative circadian rhythms of bioluminescence from *Per2* (**b**) and *Bmal1* (**c**) promoter fused to a *dLuc* reporter gene. **d**–**f**, Representative circadian rhythms of bioluminescence from wild-type (**d**) and mutant (**e**) constructs or from *SV40* promoter (**f**) fused to a *dLuc* reporter gene.

Methods

Microarray experiments

Slices (0.5 mm thick) of mouse brain were generated using Mouse Brain Matrix (Neuroscience) under LD or DD conditions, and then the SCNs were punched out bilaterally from the frozen slices under a stereomicroscope with a microdissecting needle (gauge 0.5 mm). Livers were dissected and frozen in liquid nitrogen. Total RNA was prepared from 50 pooled pairs of SCNs and four pooled livers at each time point using Trizol reagent (GIBCO BRL). Complementary DNA synthesis and cRNA labelling reactions were performed as previously described[26]. We used Affymetrix high-density oligonucleotide arrays for *Mus musculus* (Murine Genome Array U74A) version 2 for SCN expression and version 1 for liver expression profiling. Expression data and other systems-biological information used in this paper will be available at the Database for Systems Biology (http://www.dbsb.org/).

Animals

Balb/c mice (male) purchased five weeks postpartum were adapted to standard 12-h light/12-h dark cycles (LD) for two weeks before samples were obtained under LD or constant darkness (DD) conditions every 4 h starting at ZT0 (zeitgeber time zero) or CT0 over two days.

In situ hybridization

The *in situ* hybridization and method of quantification of messenger RNA have been described in detail previously[30]. Serial coronal sections (40 μm thick) of mouse brain were prepared using a cryostat. Fragments of cDNA were obtained by PCRs, which were then subcloned into PGEM-T easy vector (Promega). ^{35}S-labelled sense and antisense probes were transcribed using T7 or SP6 RNA polymerases. Antisense probes produced specific hybridization signals in the SCNs and/or other brain regions, whereas the sections hybridized with the sense probes exhibited no specific signal. The radioactivity of each section on BioMax film (Kodak) was analysed using a microcomputer interfaced to an image analysing system (MCID, Imaging Research) after conversion to relative optical density using ^{14}C-acrylic standards (Amersham). Data were normalized with respect to the difference between signal intensities in equal areas of the SCN and the corpus callosum. The optical densities of the sections from the rostralmost caudalmost portion of the SCNs (ten sections per mouse) were then summed; the sum was used as the mRNA abundance in this region. 'Relative RNA abundance' means that the peak value was adjusted to 100%.

Quantitative PCR

To verify the microarray results, quantitative PCR was performed with the ABI Prism 7700 and SYBR Green Reagents (Applied Biosystems). cDNAs were synthesized from 0.5 μg of total RNA using Superscript II reverse transcriptase (Invitrogen). Samples contained 1 × SYBR Green Master Mix, 0.5 μM primers and 1/40 synthesized cDNA in a 25 μl volume. The PCR conditions were as follows: 10 min at 95 °C, then 40 cycles of 15 s at 94 °C, 30 s at 60 °C and 1 min at 72 °C. Absolute cDNA abundance was calculated using the standard curve obtained from mouse genomic DNAs. We used GAPDH as an internal control.

Determination of transcription start sites

In order to determine TSSs, oligo-capping was performed as described previously[13] using 10 mg of polyA + RNA isolated from whole human brain, cerebellum and liver. cDNA was synthesized using a Thermoscript (Gibco BRL) from the oligo-capped mRNA and amplified by nested PCR with outer and inner 5′ primers complementary to the cap-replacing oligo sequence and outer and inner 3′ gene-specific primers. The PCR products were purified and sequenced. TSSs were identified precisely as the oligo-capped sites of the cDNAs.

Constructs

The wild-type Rev-ErbA/ROR response element and mutant Rev-ErbA/ROR response element were constructed as follows: the following oligonucleotides were inserted into the *SmaI* site of the *SV40-dLuc* vector[12]. WT:5′-GATTGGTCGGAAAGTAGGTTAGTGG TGCGACATTTAGGGAAGGCAGAAAGTAGGTCAGGGACGGAGG-3′. Mutant: 5′-GATTGGTCGGAAAGTCCTAGCGTGGTGCGACATTTAGGGAAGGCAGAAAGT CCTAGCGGGACGGAGG-3′. The constructs were verified by sequencing.

Transfection and real-time monitoring of circadian bioluminescence

Rat1-R12 cells (ATCC) were grown in Dulbecco's modified Eagle's medium supplemented with 10% fetal bovine serum (Sigma). Cells were plated at 1.0×10^6 cells per dish in 35-mm dishes 24 h before transfection. Cells were transfected with LipofectAMINE 2000 reagent (GIBCO BRL) according to the manufacturer's instructions. Cells in each dish were transfected with 1 μg (total) of expression plasmids. After 16 h, cells in each dish were treated with 0.1 μM dexamethasone (Sigma), and after 2 h these media were replaced with 2 ml culture medium (Dulbecco's modified Eagle's medium supplemented with 10% fetal bovine serum (Sigma)) supplemented with 10 mM HEPES (pH 7.2), 0.1 mM luciferin (Promega), and antibiotics (25 U ml^{-1} penicillin, 25 μg ml^{-1} streptomycin). Bioluminescence was measured with photomultiplier tube (PMT) detector assemblies (Hamamatsu). The modules and cultures were maintained in a light-tight incubator at 36 °C and interfaced to IBM PC-type computers for continuous data acquisition. The PMT was positioned about 2 cm above the culture, and photon counts were integrated over 1-min intervals.

Received 12 April; accepted 5 June 2002; doi:10.1038/nature00906.

1. King, D. P. *et al.* Positional cloning of the mouse circadian clock gene. *Cell* **89,** 641–653 (1997).
2. Bunger, M. K. *et al.* Mop3 is an essential component of the master circadian pacemaker in mammals. *Cell* **103,** 1009–1017 (2000).
3. Zheng, B. *et al.* Nonredundant roles of the mPer1 and mPer2 genes in the mammalian circadian clock. *Cell* **105,** 683–694 (2001).
4. van der Horst, G. T. *et al.* Mammalian Cry1 and Cry2 are essential for maintenance of circadian rhythms. *Nature* **398,** 627–630 (1999).
5. Lowrey, P. L. *et al.* Positional syntenic cloning and functional characterization of the mammalian circadian mutation tau. *Science* **288,** 483–492 (2000).
6. Gekakis, N. *et al.* Role of the CLOCK protein in the mammalian circadian mechanism. *Science* **280,** 1564–1569 (1998).
7. Jin, X. *et al.* A molecular mechanism regulating rhythmic output from the suprachiasmatic circadian clock. *Cell* **96,** 57–68 (1999).
8. Kume, K. *et al.* mCRY1 and mCRY2 are essential components of the negative limb of the circadian clock feedback loop. *Cell* **98,** 193–205 (1999).
9. Shearman, L. P. *et al.* Interacting molecular loops in the mammalian circadian clock. *Science* **288,** 1013–1019 (2000).
10. Yu, W., Nomura, M. & Ikeda, M. Interactivating feedback loops within the mammalian clock: BMAL1 is negatively autoregulated and upregulated by CRY1, CRY2, and PER2. *Biochem. Biophys. Res. Commun.* **290,** 933–941 (2002).
11. Kitano, H. Systems biology: a brief overview. *Science* **295,** 1662–1664 (2002).
12. Chen, W., Ueda, H. R. & Hashimoto, S. In vitro determination of clock-controlled elements. *Curr. Biol.* (submitted).
13. Maruyama, K. & Sugano, S. Oligo-capping: a simple method to replace the cap structure of eukaryotic mRNAs with oligoribonucleotides. *Gene* **138,** 171–174 (1994).
14. Clayton, J. D., Kyriacou, C. P. & Reppert, S. M. Keeping time with the human genome. *Nature* **409,** 829–831 (2001).
15. Hida, A. *et al.* The human and mouse Period1 genes: five well-conserved E-boxes additively contribute to the enhancement of mPer1 transcription. *Genomics* **65,** 224–233 (2000).
16. Paca-Uccaralertkun, S. *et al.* In vitro selection of DNA elements highly responsive to the human T- cell lymphotropic virus type I transcriptional activator. *Tax. Mol. Cell Biol.* **14,** 456–462 (1994).
17. Obrietan, K., Impey, S., Smith, D., Athos, J. & Storm, D. R. Circadian regulation of cAMP response element-mediated gene expression in the suprachiasmatic nuclei. *J. Biol. Chem.* **274,** 17748–17756 (1999).
18. Harding, H. P. & Lazar, M. A. The orphan receptor Rev-ErbA alpha activates transcription via a novel response element. *Mol. Cell Biol.* **13,** 3113–3121 (1993).
19. Jetten, A. M., Kurebayashi, S. & Ueda, E. The ROR nuclear orphan receptor subfamily: critical regulators of multiple biological processes. *Prog. Nucleic Acid Res. Mol. Biol.* **69,** 205–247 (2001).
20. Panda, S. *et al.* Coordinated transcription of key pathways in the mouse by the circadian clock. *Cell* **109,** 307–320 (2002).
21. Duffield, G. E. *et al.* Circadian programs of transcriptional activation, signalling, and protein turnover revealed by microarray analysis of mammalian cells. *Curr. Biol.* **12,** 551–557 (2002).
22. Akhtar, R. A. *et al.* Circadian cycling of the mouse liver transcriptome, as revealed by cDNA microarray, is driven by the suprachiasmatic nucleus. *Curr. Biol.* **12,** 540–550 (2002).
23. Grundschober, C. *et al.* Circadian regulation of diverse gene products revealed by mRNA expression profiling of synchronized fibroblasts. *J. Biol. Chem.* **276,** 46751–46758 (2001).
24. Storch, K. F. *et al.* Extensive and divergent circadian gene expression in liver and heart. *Nature* **417,** 78–83 (2002).
25. McDonald, M. J. & Rosbash, M. Microarray analysis and organization of circadian gene expression in *Drosophila*. *Cell* **107,** 567–578 (2001).
26. Ueda, H. R. *et al.* Genome-wide transcriptional orchestration of circadian rhythms in *Drosophila*. *J. Biol. Chem.* **277,** 14018–14052 (2002).
27. Claridge-Chang, A. *et al.* Circadian regulation of gene expression systems in the *Drosophila* head. *Neuron* **32,** 657–671 (2001).
28. Harmer, S. L. *et al.* Orchestrated transcription of key pathways in *Arabidopsis* by the circadian clock. *Science* **290,** 2110–2113 (2000).
29. Cho, R. J. *et al.* Transcriptional regulation and function during the human cell cycle. *Nature Genet.* **27,** 48–54 (2001).
30. Shigeyoshi, Y. *et al.* Light-induced resetting of a mammalian circadian clock is associated with rapid induction of the mPer1 transcript. *Cell* **91,** 1043–1053 (1997).

Supplementary Information accompanies the paper on *Nature*'s website (http://www.nature.com/nature).

Acknowledgements

We thank T. Kojima, T. Katakura and H. Urata for technical assistance. This study was performed as a part of a research and development project of the Industrial Science and Technology Program supported by NEDO (New Energy and Industrial Technology Development Organization).

Competing interests statement

The authors declare that they have no competing financial interests.

Correspondence and requests for materials should be addressed to H.R.U. (e-mail: hiro@m.u-tokyo.ac.jp) or to Y.S. (e-mail: shigey@med.kindai.ac.jp).

A re-examination of proximodistal patterning during vertebrate limb development

Andrew T. Dudley*, María A. Ros† & Clifford J. Tabin*

** Department of Genetics, Harvard Medical School, 200 Longwood Avenue, Boston, Massachusetts 02115, USA*
† Departamento de Anatomía y Biología Celular, Facultad de Medicina, Universidad de Cantabria, 39011 Santander, Espana

The 'progress zone' model provides a framework for understanding progressive development of the vertebrate limb[1]. This model holds that undifferentiated cells in a zone of fixed size at the distal tip of the limb bud (the progress zone) undergo a progressive change in positional information such that their specification is altered from more proximal to more distal fates. This positional change is thought to be driven by an internal clock that is kept active as long as the cells remain in the progress zone. However, owing to cell division, the most proximal of these cells are continually pushed outside the confines of the zone. As they exit, clock function ceases and cells become fixed with the positional value last attained while within the zone. In contrast to this model, our data suggest that the various limb segments are 'specified' early in limb development as distinct domains, with subsequent development involving expansion of these progenitor populations before differentiation. We also find, however, that the distal limb mesenchyme becomes progressively 'determined', that is, irreversibly fixed, to a progressively limited range of potential proximodistal fates.

Overlying the progress zone is a ridge of pseudostratified epithelium, known as the apical ectodermal ridge (AER), which runs along the anterior–posterior rim of the distal tip of the limb bud[2]. When the AER is removed, the limb fails to form distal structures, suggesting that patterning of the distal limb is dependent on the AER[3]. The observation that less severe truncations result when the AER is removed at progressively later stages has been taken as strong evidence in support of the progress zone model. In this context, a 'specification map' for the formation of the skeletal elements of the chick wing has been proposed on the basis of examination of truncations resulting from AER removal at various stages[4]. We noted, however, that other reports have shown that, after removal of the AER, some distal mesenchyme cells are eliminated by cell death. In particular, one study detected a region of cell death extending 200 μm from the distal tip within 4 h after AER removal at stage 22 (ref. 5). We reasoned that if this region of cell death remained constant in size at every stage, then a proportionally larger part of